



# Preferential photoassimilation of volatile fatty acids by purple non-sulfur bacteria: Experimental kinetics and dynamic modelling

Paloma Cabezas Segura<sup>a</sup>, Quentin De Meur<sup>a</sup>, Abbas Alloul<sup>b</sup>, Audrey Tanghe<sup>c</sup>,  
Rob Onderwater<sup>c</sup>, Siegfried E. Vlaeminck<sup>b</sup>, Alain Vande Wouwer<sup>d</sup>, Ruddy Wattiez<sup>a</sup>,  
Laurent Dewasme<sup>d</sup>, Baptiste Leroy<sup>a,\*</sup>

<sup>a</sup> Laboratory of Proteomics and Microbiology, University of Mons, 7000 Mons, Belgium

<sup>b</sup> Research Group of Sustainable Energy, Air and Water Technology, Department of Bioscience Engineering, University of Antwerp, Groenenborgerlaan, 2020, Antwerpen, Belgium

<sup>c</sup> Materia Nova ASBL, Parc Initialis, Avenue Copernic 3, 7000 Mons, Belgium

<sup>d</sup> Systems, Estimation, Control and Optimization Group (SECO), University of Mons, 7000 Mons, Belgium

## ARTICLE INFO

### Keywords:

Resource recovery  
Wastewater treatment  
Parameter estimation  
*Rhodospirillum rubrum*

## ABSTRACT

Purple non-sulfur bacteria (PNSB) are known for their metabolic versatility and thrive as anoxygenic photo-heterotrophs. In environmental engineering and resource recovery, cells would grow on mixtures of volatile fatty acids (VFA) generated by anaerobic fermentation of waste streams. In this study, we aim to better understand the behavior of *Rhodospirillum rubrum*, a model PNSB species, grown using multiple VFA as carbon sources. We highlighted that assimilation of individual VFA follows a sequential pattern. Based on observations in other PNSB, this seems to be specific to isocitrate lyase-lacking organisms. We hypothesized that the inhibition phenomenon could be due to the regulation of the metabolic fluxes in the substrate cycle between acetoacetyl-CoA and crotonyl-CoA. Developed macroscopic dynamic models showed a good predictive capability for substrate competition for every VFA mixture containing acetate, propionate, and/or butyrate. These novel insights provide valuable input for better design and operation of PNSB-based waste treatment solutions.

## 1. Introduction

Over the past few years, the interest in a more circular economy has been rising, suggesting that waste should be treated as secondary feedstocks, being valorized and upcycled. Following this principle, an important research and development effort was undertaken to develop sustainable environmental biotechnologies to valorize organic in wastewater or solid waste in higher added value products such as bio-fuel, bioplastics, or microbial proteins [1–3]. Purple non-sulfur bacteria (PNSB) can offer solutions to phototrophically upcycle organic resources from waste streams to several added-value compounds such as fertilizers, for feed, polyhydroxyalkanoates (PHA) for bioplastics, pigments, coenzyme Q10 or H<sub>2</sub> [4–6]. Nevertheless, waste streams contain usually a mixture of carbon compounds such as polysaccharides, fatty acids, DNA, or polyphenolic structures which make it challenging to develop a universal, robust and reproducible process [7]. Conversion of such complex organic matrices, for instance through fermentation, into

simpler molecules such as volatile fatty acids (VFAs), is a way to increase the process feasibility and transferability. VFAs can then be subsequently easily assimilated by organisms such as PNSB [8]. The most found VFAs in fermented waste streams are acetate, butyrate, iso-butyrate, propionate, valerate, and isovalerate. Even though, the VFA speciation depends on many factors such as substrate, temperature, pH, or hydraulic and solid retention times, the most abundant produced VFAs being usually acetate, butyrate, propionate, and valerate [9–14].

For the synthesis of PHA in PNSB, a precise understanding of the assimilation processes of VFAs is required as the carbon source used to support the bacterial growth directly impacts the composition of the polymer [15,16]. In this frame, some mathematical models were developed to describe the assimilation in microbial cultures of some volatile fatty acid mixtures [17–21]. Substrate uptake rate varies significantly depending on the composition of the mix and, in addition, the biomass may exhibit some substrate consumption preferences. It was, for instance, observed that *Plasticumulans acidivorans* preferentially consume butyrate over acetate [19]. Therefore, the development

\* Correspondence to: Laboratory of Proteomic and Microbiology, UMONS, Avenue du champs de Mars, 6 (Pentagone 3B), 7000, Mons, Belgium.

E-mail address: [baptiste.leroy@umons.ac.be](mailto:baptiste.leroy@umons.ac.be) (B. Leroy).

<https://doi.org/10.1016/j.bej.2022.108547>

Received 21 March 2022; Received in revised form 8 July 2022; Accepted 18 July 2022

Available online 21 July 2022

1369-703X/© 2022 Elsevier B.V. All rights reserved.

### Nomenclature

$\mu_{\max_{\text{ace}}}$ ,  $\mu_{\max_{\text{prop}}}$ ,  $\mu_{\max_{\text{val}}}$ ,  $\mu_{\max_{\text{but}}}$ ,  $\mu_{\max_{\text{VFA}}}$ ,  $\mu_{\max}$  maximal uptake rates ( $\text{h}^{-1}$ ).  
 $K_{\text{ace}}$ ,  $K_{\text{prop}}$ ,  $K_{\text{but}}$ ,  $K_{\text{val}}$  half-saturation constants (g/g).  
 $K_{i_{\text{ace}}}$ ,  $K_{i_{\text{prop}}}$ ,  $K_{i_{\text{prop+ace}}}$  inhibition constants (g/l).  
 $C_{\text{ace}}$ ,  $C_{\text{prop}}$ ,  $C_{\text{but}}$ ,  $C_{\text{val}}$ ,  $C_{\text{hb}}$ ,  $C_{\text{hv}}$ ,  $h_{b_c}$ ,  $h_{v_c}$  substrate to biomass yield coefficients (g/g).  
 [Ace], [Prop], [But], X concentrations of acetate, propionate, butyrate and biomass.

of such a model requires the observation and understanding of the microbial strain metabolic behavior in presence of different VFA mixtures, as well as an insight into the metabolic pathways involved in their assimilation.  $\text{C}_2$  compounds such as acetate are usually assimilated through the glyoxylate shunt [22]. However, some PNSB are lacking the isocitrate lyase (ICL<sup>-</sup> organisms) which is the key enzyme of this pathway. In this case, the net assimilation of  $\text{C}_2$  compounds requires the use of alternative anaplerotic pathways. The ethylmalonyl-CoA (EMC) pathway has been proposed as a key alternative pathway to fulfill this role in several ICL<sup>-</sup> PNSB including *Rs. rubrum* [23–25] (Fig. S2). In *Rs. rubrum*, the propionyl-CoA resulting from the EMC is first carboxylated in methylmalonyl-CoA before being converted to succinate [23–25]. When propionate is used as a carbon source, its assimilation equivalently occurs via methylmalonyl-CoA [26] (Fig. S2). The assimilation of butyrate ( $\text{C}_4$ ) under photoheterotrophic conditions, remains poorly described even though this molecule is known to support photoheterotrophic growth in most of the PNSB. A recent study carried out in our lab on *Rs. rubrum* has underlined the use of the EMC pathway for butyrate assimilation but also of the newly proposed methylbutanoyl-CoA (MBC) pathway [27] (Fig. S2). Most studies performed with PNSB to better characterize the photoheterotrophic assimilation pathways of VFAs were achieved on cell cultures supplied with a unique carbon source. From that perspective, the obtained data can only result in a metabolic adaptation to the defined carbon source which can significantly affect metabolism and genome as we recently demonstrated in the context of the long-term adaptation of *Rs. rubrum* to the assimilation of acetate [28]. However, when referring to an environmental context but also an industrial application where waste streams are used as substrates, the probability that PNSB grows with a unique carbon source is fairly low. Some studies already highlighted a synergic effect on the uptake rate of VFAs or a delay in this uptake when VFAs were simultaneously present in the medium using PNSB [5,6].

This study aims to experimentally unravel the simultaneous uptakes pattern of individual VFAs in a mixture using *Rs. rubrum* as a model organism and to propose a mathematical model able to describe such phenomenon. In addition, the PNSB *Rhodobacter capsulatus*, and *Rhodobacter sphaeroides*, often retrieved in open communities for wastewater treatment were also investigated regarding their assimilatory behavior for blends of VFAs.

## 2. Materials and methods

### 2.1. *Rs. rubrum* tests: strain and culture conditions

*Rhodospirillum rubrum* S1H (ATCC15903) is grown in a medium used for photoheterotrophic culture conditions, that is based on the basal salt medium of Segers & Verstraete described by Suhaimi et al. [29,30], supplemented with  $\text{NH}_4\text{Cl}$  (35 mM) as the nitrogen source,  $\text{NaHCO}_3$  (3 mM or 50 mM), and biotin (0.06 mM). Six different mixtures of VFAs were used as carbon sources: [1] acetate (35 mM), butyrate (10 mM) and propionate (5 mM) in the 7:4:1.5 carbon ratio [2], acetate (31 mM) and propionate (20.6 mM) [3], acetate (31 mM) and butyrate (15.5 mM) [4],

propionate (20.6 mM) and butyrate (15.5 mM), and [5] acetate (12 mM) and butyrate (15.5 mM) [6], propionate (15 mM) and butyrate (15.5 mM). Mixtures [2–4] have a carbon ratio between VFAs of 1:1. Succinate (31 mM) was used as carbon source in control conditions, at the same net carbon concentration (124 mM). The pH was adjusted to 6.9. *Rs. rubrum* was grown under anaerobic phototrophic conditions in 50 ml sealed serum flasks under  $50 \mu\text{mole}\cdot\text{m}^{-2}\cdot\text{s}^{-1}$  of light intensity supplied by halogen lamps (Sencys; 10 W; 100 lumens; 2650 K), at  $30^\circ\text{C}$  with a rotary shaking at 200 rpm. Each culture condition was achieved with five biological replicates, except for the cultivation experiments. Nitrogen gas was used to purge oxygen from the upper gas phase and the flasks were hermetically sealed. The cultures were inoculated at a starting  $\text{OD}_{680\text{nm}}$  between 0.4 and 0.5 and the growth was monitored following the turbidity at  $\text{OD}_{680\text{nm}}$ . A correlation curve between OD and biomass dry weight was used to convert  $\text{OD}_{680\text{nm}}$  in biomass content.

### 2.2. *Rs. rubrum* tests: monitoring of VFAs consumption

The monitoring of *Rs. rubrum* VFA consumption was performed on culture supernatants obtained by centrifugation at 16,000 g for 10 min at  $4^\circ\text{C}$  and stored at  $-20^\circ\text{C}$  before analysis. Aliquots (100  $\mu\text{L}$ ) of culture supernatant were analyzed by HPLC-refractometry (Waters 2695 separation Module; Waters 2414 Refractive Index Detector). The separation was done in isocratic mode using a Shodex Sugar SH1011 column (300 mm  $\times$  8 mm) with 5 mM  $\text{H}_2\text{SO}_4$  as the mobile phase. The amounts of acetate, propionate, butyrate, and succinate were determined by integrating their specific peaks and comparing area under the curve with external standards.

### 2.3. *Rb. sphaeroides* and *Rb. capsulatus* tests: strains, culture conditions, and analytical methods

*Rhodobacter sphaeroides* (LMG 2827), *Rhodobacter capsulatus*, and an enriched community which was dominated by 80 % by *Rhodobacter capsulatus* were used as bacterial strains to extend the study to other PNSB. Batch experiments involving *Rhodobacter sphaeroides* and *Rhodobacter capsulatus* were carried out in 500 ml Erlenmeyer with a working volume of 500 ml in triplicates and closed with a screw cap containing a silicone rubber polytetrafluoroethylene protected septum (Duran, Germany). The headspace was flushed for 1 min with nitrogen gas. Stirring was performed with a multipoint stirrer at 300 rpm (Thermo Scientific, USA). The batch experiment for *Rb. sphaeroides* was performed in a climate chamber (Snijders Scientific) at  $28^\circ\text{C}$  equipped with 36 W fluorescent lamps (Sylvania, Germany) at a light intensity of  $30 \text{ W m}^{-2}$ . The batch test for the enriched *Rb. capsulatus* was tested at  $29 \pm 1^\circ\text{C}$ , illuminated with 500 W halogen lamps (Philips, Netherlands) at a light intensity of  $30 \text{ W m}^{-2}$ , and covered with infrared transmission filters (Bay Plastics, UK). Samples of 10 ml were taken for further analyses and to monitor the growth spectrophotometrically at 660 nm. VFAs were analyzed by High-Performance Liquid Chromatography (Agilent technologies 1200) coupled with a diode array detector (210 nm), a Bio-Rad Aminex® column (300 mm 7,8 mm) with Bio-Rad Micro-Guard Cation H Refill Cartridges and a column temperature of  $40^\circ\text{C}$ . The samples were injected into 50 mM  $\text{H}_2\text{SO}_4$  (Honeywell Fluka™) in deionized water (Arium® 611) with an injection volume of 20  $\mu\text{L}$  and a sample flow rate of  $0.6 \text{ ml min}^{-1}$ .

### 2.4. Statistical analysis on biological experiments

All graphs were plotted using the software GraphPad Prism (Version 6.01). The results were reported as the means and standard deviations computed by GraphPad Prism 6.01. To evaluate the significance of changes, *t*-tests or ANOVA were performed with a threshold set at 0.05. Significance difference was marked using different lower cases. These analyses were performed using MATLAB software (version R2018a 9.4.0.813654).

## 2.5. Mathematical model identification procedure

The proposed modeling approach is based on a priori knowledge of the metabolic network and data obtained from the in-lab experiments described in Section 3.2. The considered bioprocess can be described by the following macroscopic reaction scheme:



with  $k \in [1, M]$  where  $M$  is the number of reactions,  $\mathbb{R}_k$  and  $\mathbb{P}_k$  denote respectively the set of reactants and products in the reaction  $k$ . The parameters  $k_{i,k}$  and  $k_{j,k}$  are pseudo stoichiometric coefficients while  $\varphi_k$  is the corresponding reaction rate. Applying mass balance to (1), the following ordinary differential equation (ODE) system is obtained, describing the variations of each species concentration with time:

$$\frac{d\xi(t)}{dt} = K \varphi(\xi, \theta_\varphi, t) \quad (6.2)$$

where  $K$  is the pseudo-stoichiometric matrix and  $\theta_\varphi$  the kinetic parameters. Parameter estimation is conducted by minimizing a least-squares criterion measuring the distance between model-simulated data  $\xi_m$  and experimental measurements  $\xi_{\text{exp}}$  as in:

$$J(\theta) = (\xi_m(\theta) - \xi_{\text{exp}})^T Q^{-1} (\xi_m(\theta) - \xi_{\text{exp}}) \quad (6.3)$$

where  $\theta$  is the parameter vector (gathering stoichiometric and kinetic parameters).

The initial state  $\xi_0$  is a vector of length  $N$  times  $n_{\text{exp}}$ ,  $n_{\text{exp}}$  being the number of used experiments and  $N$  the size of vector  $\xi$ , that is, the number of studied macroscopic species (in the current case, biomass and VFAs).  $\xi_{0,0}$  is guessed using the experimental measurements at time  $t = 0$ .  $Q$  is the measurement error covariance matrix designed as a diagonal matrix (assuming independent distributions of the measurement errors) containing the squares of the maximum concentration levels of each species, a good practice rule to normalize the distances calculated in (3) when the error distributions are not assumed to be known a priori. Parameter identification is performed with the MATLAB optimizer “fmincon” which uses an interior point method and tolerates upper and lower bounds on the assumed unknown parameters, allowing to reduce the search space and accelerate the optimization. The latter option can indeed be achieved since, for most of the kinetic and stoichiometric parameters, the general order of magnitude can be easily guessed from previous studies, or some trivial data analyzes.

The data sets obtained from three biological replicates are used for each substrate operating condition (VFAs mixture) for parameter estimation and model direct validation. Supplementary data coming from a separate experiment are used for model cross-validation. Local parameter identifiability and sensitivity analysis are addressed based on the Fisher Information Matrix (FIM), which can be computed as follows:

$$\text{FIM} = \sum_{tk=1}^{n_{\text{meas}}} (\xi_{\theta,i}(t_k, \hat{\theta}))^T Q^{-1} \xi_{\theta,i}(t_k, \hat{\theta}) \quad (6.4)$$

where  $t_k$  is the sampling time and  $n_{\text{meas}}$  is the number of samples. An estimate of the parameter estimation error covariance matrix can be obtained from the Cramer-Rao bound as follows:

$$\hat{P} > \sigma^2 \text{FIM}^{-1} \quad (6.5)$$

with  $\sigma^2$  being the a posteriori estimate of the measurement error variance calculated from the residual cost function at the optimum:

$$\sigma^2 = \frac{J^*}{n_{\text{exp}} * N_{\text{meas}} - n_\theta} \quad (6.6)$$

where  $N_{\text{meas}}$  is the total number of measurements ( $n_{\text{meas}}$  times  $N$ ) and  $n_\theta$

is the number of estimated parameters. Model fitting is assessed by the root mean square error (RMSE).

## 3. Results and discussion

In this first experimental study, the composition of the mixture of VFAs and the proportion of each component was based on the composition of the effluents of a thermophilic anaerobic fermentation pilot plant operated in the context of the micro-ecological life support system alternative MELiSSA program from ESA [31]. *Rs. rubrum* was first grown in a culture medium supplemented with a mixture of VFAs containing acetate, butyrate, and propionate in a 7:4:1.5 carbon ratio and 3 mM of bicarbonate. The growth rate in the control (succinate) and the VFAs mixture conditions did not show any significant difference but for the same nominal 124 mM of carbon present in the medium, the biomass level reached at the end of the culture was higher with the mixture of VFAs than in the control condition (Fig. 1).

### 3.1. Delayed butyrate uptake in presence of acetate and propionate

Unexpectedly, while the use of acetate as a single carbon source under photoheterotrophic conditions with low bicarbonate levels is characterized by a long lag phase (100 h) [28] (Fig. S1), we observed that both the growth and the acetate assimilation started without delay with a VFA mixture largely dominated by acetate. The monitoring of the VFA concentrations in the culture medium during the growth showed that acetate assimilation rate was high from the beginning of the experiment. The assimilation rate of propionate was low during the first days and then quickly increased. For butyrate, on the other hand, the assimilation rate was low until day 1.5 and increased only after the complete assimilation of propionate and a significant decrease of acetate concentration (Fig. 1). The VFA consumptions followed a sequential pattern of assimilation, butyrate being significantly consumed essentially at the end of the experiment.

### 3.2. Butyrate assimilation is delayed by the presence of acetate and/or propionate

To define if acetate or propionate inhibits assimilation of butyrate, *Rs. rubrum* was grown in a culture medium supplemented with 3 different binary mixtures each containing only two of the three VFAs in the same equivalent net carbon concentrations (for a total of 124 mM net of carbon) and 3 mM of bicarbonate (Fig. 2). Culture of *Rs. rubrum* using acetate, propionate, butyrate as sole carbon source were used as controlled (Fig. S1). To confirm the absence of deleterious interaction

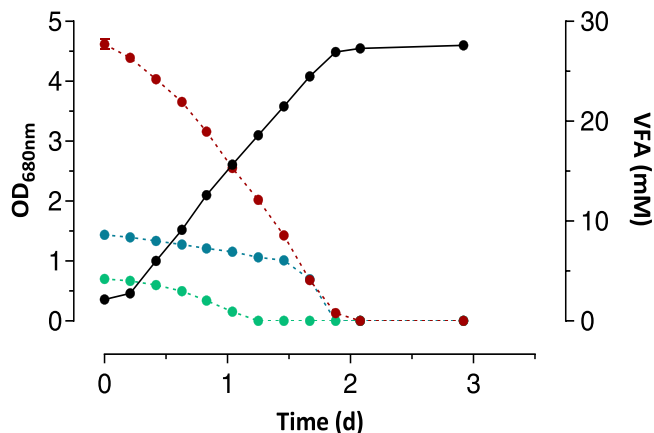


Fig. 1. Monitoring of the growth (●) and VFA consumptions in cultures of *Rs. rubrum* cultivated with a mix of acetate (●), propionate (●), and butyrate (●) as carbon sources (7:4:1.5 carbon ratio).

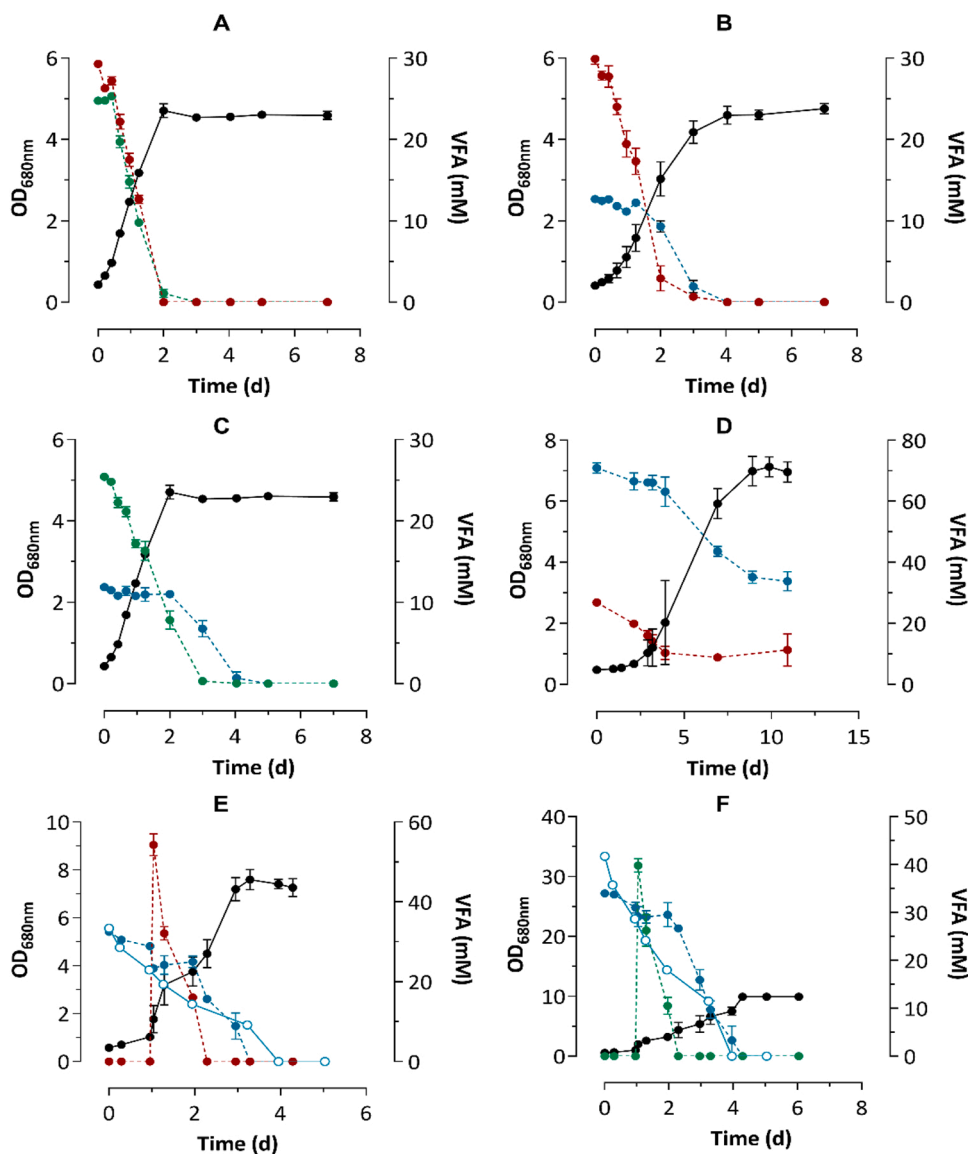


Fig. 2. Monitoring of the growth and VFA consumptions in cultures of *Rs. rubrum* S1H cultivated in binary mixtures of VFAs: (A) acetate and propionate ( $n = 3$ ), (B) acetate and butyrate ( $n = 3$ ), (C) propionate and butyrate ( $n = 3$ ), (D) acetate with an excess of butyrate ( $n = 3$ ), (E) butyrate and spike of acetate ( $n = 3$ ), (F) butyrate and spike of propionate ( $n = 3$ ). The production of biomass (●) and the concentration of acetate (●), butyrate (●), and propionate (●) are presented. Control with consumption of butyrate by *Rs. rubrum* in presence of 50 mM of bicarbonate (○).

observed here before, the assimilation profile of a mixture of acetate and propionate was first explored. Both VFAs were simultaneously consumed during the growth phase and propionate could be completely assimilated with the 3 mM of bicarbonate supplemented to the medium (Fig. 2A). Considering the assimilation pathways of propionate [26] and acetate [24] in *Rs. rubrum*, this observation appeared to be quite logical since the propionyl-CoA is a metabolic intermediate of the ethylmalonyl-CoA pathway used to photoassimilate acetate.

Regarding the assimilation of a mixture of acetate and butyrate, no lag-phase and no dependency on bicarbonate supplementation were observed in the growth (Fig. 2B). Similar observations could be made on the culture growing with propionate and butyrate as carbon sources (Fig. 2C). In both cases, butyrate consumption was delayed until the concentration of the other VFA has dropped down. To confirm this observation, the assimilation rates of each VFA at different steps of the growth period were calculated (Fig. 3). It can be observed that when VFAs are alone or in a mixture in which no sequential assimilation is observed, as, in the case of a mixture of acetate and propionate, no change in the assimilation rate is observed along the biomass growth period. In contrast, a significant difference in the VFA uptake is observed

in a mix exhibiting their sequential assimilation (Fig. 3). In the case of the mixture of acetate and butyrate, it can be noticed that while at the beginning of the culture acetate has a significantly higher uptake rate than butyrate, during the second part of the cultivation the opposite phenomenon is observed (Fig. 3). Similar observations can be made for the mixture of propionate and butyrate or the mixture of acetate, propionate, and butyrate. This tends to confirm the sequential assimilation of VFAs when butyrate is assimilated in presence of acetate or propionate. A fifth mixture was used containing acetate (25 mM) and excess butyrate (70 mM). In the medium containing this mixture, the  $\text{NH}_4\text{Cl}$  concentration was adjusted to 85 mM according to the net carbon concentration (330 mM) to respect the C/N ratio.

To determine if the observed phenomenon is ruled by the concentration levels of acetate and butyrate, *Rs. rubrum* was cultivated with a medium supplemented with acetate and butyrate in a carbon ratio of 1:5, respectively. Despite the excess of butyrate in the culture medium, the preferential assimilation of acetate over butyrate is still appearing (Fig. 2D), suggesting that this mechanism is not related to the higher concentration of acetate. It is worth noting that acetate assimilation rate was lower in this condition which is unexplained today and should

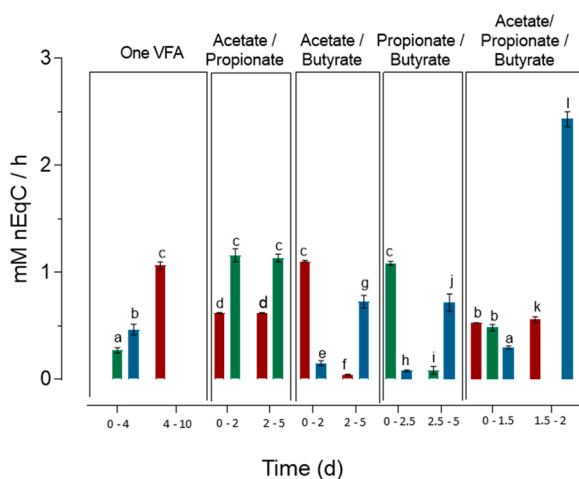


Fig. 3. Substrate consumption rate during the different phases of culture of *Rs. rubrum* using acetate (■), propionate (■), butyrate (■), or a mixture of those VFAs as a carbon source. Lower case marked significant difference ( $p$ -value  $< 0.05$ ;  $n = 3$ ).

require further investigation. As expected from the higher net carbon concentration, the culture reached very high biomass levels. Nevertheless, the growth stopped before the complete assimilations of butyrate and acetate. Considering that the carbon/nitrogen balance has been conserved in medium preparation, the depletion of other compounds such as phosphorus may explain this phenomenon. To test whether or not the latter could be linked to a substrate preference, acetate and propionate were supplemented in the medium during the exponential phase of culture initially growing on butyrate as the main carbon source (Fig. 2E and F). Culture growing with butyrate as the sole carbon source required excess of bicarbonate to grow therefore those experiments were carried with 50 mM of bicarbonate in the culture medium. As shown in Fig. 2E and F, butyrate assimilation stopped when acetate or propionate spikes occurred, indicating a possible substrate preference or inhibition at an enzymatic level. This inhibition seemed, however, to be limited to high acetate concentrations since butyrate assimilation started before the complete consumption of acetate. The inhibitory effect of acetate on butyrate assimilation could, in some way, be expected. For their assimilation, acetate and butyrate share some metabolic intermediates between acetyl-CoA and crotonyl-CoA as well as the ethylmalonyl-CoA pathway.

When acetate is the carbon source, acetyl-CoA is converted into crotonyl-CoA, while the latter serves as a substrate to produce acetyl-CoA when *Rs. rubrum* grows on butyrate (Fig. S2). The resulting metabolic mismatch is mainly related to the differential expression of two enzymes. The first one, Rru\_A3079, specific to the photoassimilation of butyrate, catalyzes the conversion of the (S)-3-hydroxybutyryl-CoA into acetoacetyl-CoA. This enzyme has been observed to be up-regulated in butyrate condition (fold change: 1.9,  $P$ -value:  $5e-8$ ) [27], and down-regulated in acetate condition (fold change: 0.3,  $P$ -value:  $4e-4$ ) [24]. The second enzyme, Rru\_A0273, is involved in the acetate assimilation and is responsible for the conversion of acetoacetyl-CoA into (R)-3-hydroxybutyryl-[28]. It is strongly downregulated in butyrate conditions (fold change: 0.3,  $P$ -value:  $4e-7$ ) [27]. Moreover, the data obtained from a mutant fitness assay performed on a transposon mutant library of *Rs. rubrum* S1H showed that the gene Rru\_A2964, coding for the enzyme catalyzing the interconversion of the crotonyl-CoA and the (R)-3-hydroxybutyryl-CoA, is essential for the strain survival under acetate condition [28], whereas the mutations knocking this gene out appeared to be beneficial in butyrate condition. Depending on the available carbon source, the bacterium seems therefore to differentially regulate the expression of two routes, avoiding a cycle between acetoacetyl-CoA and crotonyl-CoA. Interestingly, Rru\_A1835, the

enzyme involved in the conversion of the butyryl-CoA into crotonyl-CoA (and therefore directly responsible for the entry of the butyrate in the central metabolism), is strongly downregulated by acetate (fold change: 0.2,  $P$ -value:  $2e-4$ ) [24], whatever the initial concentration of butyrate (Fig. S2).

The inhibitory effect of acetate is therefore maybe not only the result of a metabolic mismatch but could also result from direct regulation of the expression of enzymes specifically related to the butyrate photo-assimilation. The inhibitory effect of propionate on the assimilation of butyrate is more difficult to interpret. As propionyl-CoA is an intermediate of both the EMC and MBC pathways, being probably both used for the butyrate assimilation [27], it could be hypothesized that its presence in high quantity could induce negative feedback on those upstream metabolic pathways, preventing the butyrate assimilation (Fig. S2). Alternatively, one could also hypothesize that the downregulation of the expression of genes required for butyrate assimilation is due to metabolites that are both produced during acetate and propionate assimilation.

### 3.3. Sequential VFA uptake is restricted to ICL- organisms

To compare VFA assimilation patterns in *Rs. rubrum* with other strains of PNSB, *Rhodobacter sphaeroides*, *Rhodobacter capsulatus*, and an enriched non-axenic culture holding *Rhodobacter capsulatus* as the majoritarian strain was grown on a mixture of volatile fatty acids containing acetate, propionate, and butyrate. Monitoring of VFA consumptions by *Rhodobacter sphaeroides* highlighted an assimilation pattern similar to what was observed in *Rs. rubrum* (Fig. 4A) with butyrate being assimilated at high rate only after concentration of acetate and propionate decreased. In *Rh. sphaeroides*, there was a clear delay in butyrate assimilation which was not consumed before day 1. Conversely, VFAs were almost simultaneously assimilated (Fig. 4B) by *Rb. capsulatus* and no phase of “low-rate” assimilation of butyrate could be observed. For the enriched non-axenic culture holding *Rhodobacter capsulatus* as majoritarian strain (Fig. 4C), a very short phase of low-rate assimilation of butyrate was observed, but the assimilation rate of butyrate quickly increased not waiting for full consumption of acetate and butyrate as observed for *Rh. sphaeroides*. The sequential assimilation of VFAs, with high rate assimilation of butyrate being observed only when acetate/propionate concentration dropped, could therefore be a characteristic of ICL organisms such as *Rs. rubrum* and *Rb. sphaeroides* that are known to depend on the EMC pathway for the assimilation of acetate. The possible metabolic mismatch described before could also explain why only ICL organisms which rely on the EMC pathway for the assimilation of acetate are unable to concomitantly assimilate acetate and butyrate. On the other hand, microorganisms using the glyoxylate shunt for acetate assimilation can simultaneously assimilate butyrate, as observed for *Rh. capsulatus* in the present study.

### 3.4. Development of a dynamic model describing *Rs. rubrum* substrate uptake preferences from a mixture of VFAs

The aim is to develop the simplest mathematical mode that described a pattern of assimilation of VFA by *Rs. rubrum* based on the experimental data presented and proteomic analysis carried in mixture production and presented in Cabecas-Segura et al. [32]. To do so, the first step is to formulate a hypothesis on the kinetic structure. In a second step, it must be ensured that all the phenomena assumed to be present in the data sets are significantly identifiable in practice, proceeding to a practical parametric identifiability analysis. If the latter does not provide satisfactory results, the factors containing the non-identifiable parameters should be removed, or new data better highlighting the corresponding phenomenon should be considered. In this case, if the confidence interval of the parameter is too wide, the model will be reduced.

In the case of the assimilation of multiple VFAs by *Rs. rubrum*, two different scenarios that are the concomitant and the sequential

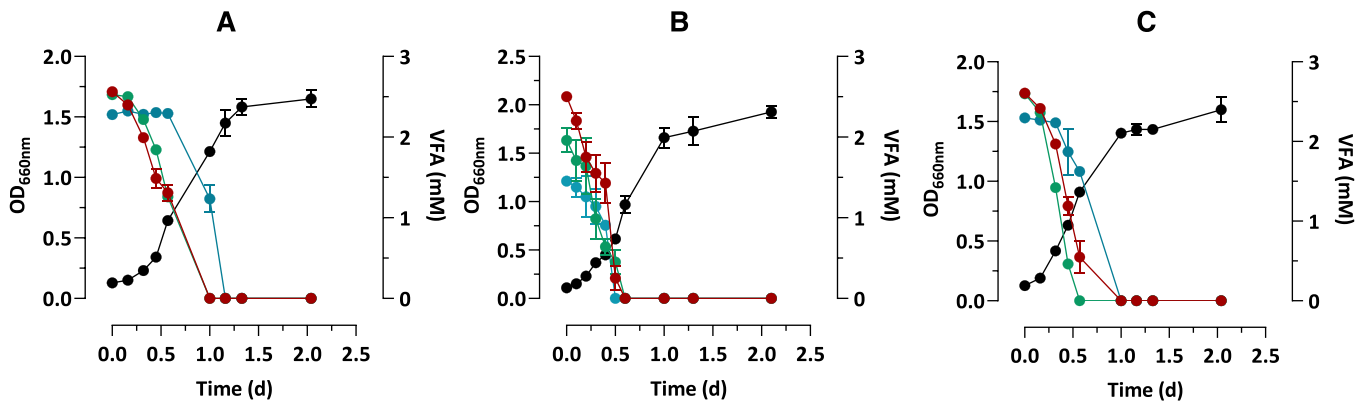


Fig. 4. Monitoring of the growth (●) and VFA consumption in batch cultures of multiple purple bacteria cultivated in an Erlenmeyer with acetate(●), butyrate (●), and propionate(●) as carbon source. Cultures of (A) *Rb. sphaeroides*, (B) *Rb. capsulatus* and (C) an enriched culture of *Rb. Capsulatus*.

assimilation of VFAs must be considered. As such different kinetic structures will be tested to describe those phenomena the corresponding mass balance are presented in Supplementary data in Table S1. The precision of the several proposed models will be assessed based on the residual of the cost function (J) as defined in (3). To describe the assimilation of VFAs that do not exhibit any preferential uptake effect, such as acetate and propionate, a first model is proposed, considering their assimilations via distinct metabolic pathways (Table 1). As reported in Table 2, the resulting fitting is satisfactory when acetate and propionate are used as substrates ( $J=0.25$ ). However, it is not the case when acetate and butyrate are used as carbon sources ( $J=6.49$ ). Various kinetic models were thus tested to describe the sequential assimilation of VFAs, namely a discontinuous switch from one VFA consumption to the other (Table S.2 β) or the introduction of an inhibition factor (Table S.2 γ). The best-predicting model considers the inhibition of butyrate assimilation by acetate as indicated by the optimization residual reported in Table S.3. This kinetic structure could be extended to the scenario using propionate and butyrate as carbon sources ( $J=0.23$ ) and to three VFA mixtures with a double inhibition phenomenon ( $J=0.42$ ). This tends to corroborate the hypothesis formulated earlier stating that the sequential assimilation is due to an inhibition phenomenon at the enzymatic level rather than a switch from a carbon source to another. The addition of an inhibition factor to the kinetic structure of VFA uptake has notably already been proposed to explain comparable phenomena occurring at the enzymatic level [21].

The second step in the development of the mathematical model is to

**Table 1**  
Selected kinetic structure to describe the assimilation of multiple VFAs by *Rs. rubrum*.

Case	Carbon source 1	Carbon source 2
Mix acetate propionate Case A.1	$\varphi_1 = X \cdot \mu_{\max Ace} \cdot \frac{[Ace]}{K_{Ace} + [Ace]}$	$\varphi_2 = X \cdot \mu_{\max Prop} \cdot \frac{[Prop]}{K_{Prop} + [Prop]}$
Mix acetate butyrate Case B.1	$\varphi_1 = X \cdot \mu_{\max Ace} \cdot \frac{[Ace]}{K_{Ace} + [Ace]}$	$\varphi_2 = X \cdot \mu_{\max But} \cdot \frac{[But]}{K_{But} + [But]} \cdot \frac{K_{iAce}}{K_{iAce} + [Ace]}$
Mix propionate butyrate Case C.1	$\varphi_2 = X \cdot \mu_{\max Prop} \cdot \frac{[Prop]}{K_{Prop} + [Prop]}$	$\varphi_2 = X \cdot \mu_{\max But} \cdot \frac{[But]}{K_{But} + [But]} \cdot \frac{K_{iProp}}{K_{iProp} + [Prop]}$
Mix acetate propionate butyrate Case D.1	$\varphi_1 = X \cdot \mu_{\max Ace} \cdot \frac{[Ace]}{K_{Ace} + [Ace]}$	$\varphi_2 = X \cdot \mu_{\max Prop} \cdot \frac{[Prop]}{K_{Prop} + [Prop]} \cdot \frac{K_{iAce}}{K_{iAce} + [Ace]}$
	<b>Carbon source 3</b>	
	$\varphi_3 = X \cdot \mu_{\max But} \cdot \frac{[But]}{K_{But} + [But]} \cdot \frac{K_{iAce}}{K_{iAce} + [Ace]} \cdot \frac{K_{iProp}}{K_{iProp} + [Prop]}$	

ensure the parametric identifiability which will be assessed via the calculation of the 95 % confidence intervals inferred from the Fisher Information Matrix (FIM) in (5). The confidence intervals related to the first proposed models are not acceptable regarding the VFA maximum uptake rates ( $\mu_{\max}$ ) (Table 2). Different model reductions not presented here were achieved. However, only the application of a sole and identical maximum uptake rate for all carbon sources of the culture medium (Table 3) led to the obtention of parameter estimations with acceptable confidence intervals (Table 4). Network interconnections between the assimilation pathways of each substrate could explain this phenomenon observed at the macroscopic level.

Indeed, propionyl-CoA and acetyl-CoA share a common metabolic assimilation pathway as propionyl-CoA is the final product of the EMC, i. e. the anaerobic pathway involved in acetyl-CoA assimilation [24,33]. Therefore acetyl-CoA and propionyl-CoA assimilations occur via the same metabolic road, that converts propionyl-CoA in succinyl-CoA via a methylmalonyl intermediate before it enters into the TCA cycle [24,33]. In addition, the assimilation of butyrate occurs via the EMC and the MBC pathways which exhibit propionyl-CoA and acetyl-CoA as intermediates. Therefore, it can be assumed that the maximum rates of acetate, propionate and butyrate assimilations could be the same.

Regarding the mixture of three VFAs, the inhibition parameters present large confidence intervals (Table 4). This could be explained by the fact that propionate and acetate are simultaneously assimilated and as such, it is not possible to differentiate the specific inhibition induced by each substrate separately. The same observation can be made regarding the saturation constants. A model reduction is therefore proposed, removing one saturation and one inhibition constant. All the resulting possible combinations were tested, and the results of the parameter estimations are presented in Supplementary data in Table S.4. This model reduction improves the fitting but provides a poor sensitivity of the inhibition and saturation constants, which induces a probable over-parametrization (Table S.4). Unfortunately, no contributive information from the metabolic pathways allows discriminating among the several possibilities to suppress inhibition or saturation constants.

This is comparable to the phenomenon observed during model development for the description of the uptakes of acetate and propionate. A model describing the uptakes of acetate, butyrate, and propionate considering butyrate on one hand, and a combination of acetate and propionate, on the other hand, was thus challenged (Table 5). Interestingly, the resulting fitting is the best and the parameter estimation is also the most accurate even if the inhibition constant still presents a relatively poor sensitivity which can be explained by its relatively low value, therefore difficult to identify with the available data (Table 6).

In Fig. 5 are presented in the measured data and the respective predictions of the calibrated models describing scenarios A.2, A.3, B.2, C.2, D.2, and D.3 that exhibit both good fitting and satisfactory

**Table 2**  
Parameter estimations and their confidence intervals for several models describing the assimilations of VFA mixtures.

Case	Mix acetate propionate (A.1)		Mix acetate butyrate (B.1)		Mix propionate butyrate (C.1)		Mix acetate propionate butyrate (D.1)	
	Value	CI (%)	Value	CI (%)	Value	CI (%)	Value	CI (%)
$\mu_{maxAce}$	0.08	108	0.13	114	–	–	2.11	6
$\mu_{maxProp}$	0.04	238	–	–	0.02	730	–	–
$\mu_{maxBut}$	–	–	0.03	488	0.02	884	0.04	371
$K_{ace}$	0.99	9	1.24	11	–	–	0.13	98
$K_{prop}$	0.32	26	–	–	0,1	167	17.96	10
$K_{but}$	–	–	0.04	339	0,2	80	0.71	18
$Ki_{ace}$	–	–	0.73	20	–	–	2.38	5
$Ki_{prop}$	–	–	–	–	0.22	74	0.02	653
$C_{ace}$	0.85	10	0.82	18	–	–	0.51	25
$C_{prop}$	2.02	4	–	–	1.22	13	0.45	28
$C_{but}$	–	–	0.37	40	3.44	5	1.10	11
J	0.25	–	0.42	–	0.23	–	0.42	–

**Table 3**  
Kinetic structures to describe the assimilations of multiple VFAs by *Rs. rubrum* after model reduction.

	Carbon source 1	Carbon source 2
Mix acetate propionate Case A.2	$\varphi_1 = X \cdot \mu_{maxAce+Prop} \frac{[Ace]}{K_{Ace} + [Ace]}$	$\varphi_2 = X \cdot \mu_{maxAce+Prop} \frac{[Prop]}{K_{Prop} + [Prop]}$
Mix acetate butyrate Case B.2	$\varphi_1 = X \cdot \mu_{maxAce+but} \frac{[Ace]}{K_{Ace} + [Ace]}$	$\varphi_2 = X \cdot \mu_{maxAce+But} \frac{[But]}{K_{But} + [But]} \frac{[Ace]}{Ki_{Ace} + [Ace]}$
Mix propionate butyrate Case C.2	$\varphi_2 = X \cdot \mu_{maxProp+But} \frac{[Prop]}{K_{Prop} + [Prop]}$	$\varphi_2 = X \cdot \mu_{maxProp+But} \frac{[But]}{K_{But} + [But]} \frac{[Prop]}{Ki_{Prop} + [Prop]}$
Mix acetate propionate butyrate Case D.2	$\varphi_1 = X \cdot \mu_{max3VFA} \frac{[Ace]}{K_{Ace} + [Ace]}$	$\varphi_2 = X \cdot \mu_{max3VFA} \frac{[Prop]}{K_{Prop} + [Prop]}$
	<b>Carbon source 3</b>	
	$\varphi_3 = X \cdot \mu_{max3VFA} \frac{[But]}{K_{But} + [But]} \frac{[Ace]}{Ki_{Ace} + [Ace]} \frac{[Prop]}{Ki_{Prop} + [Prop]}$	

**Table 4**  
Parameter estimations and their confidence intervals for several models describing the assimilations of VFA mixtures after model reduction.

Case	Mix acetate propionate (A.1)		Mix acetate butyrate (B.2)		Mix propionate butyrate (C.2)		Mix acetate propionate butyrate (D.2)	
	Value	CI (%)	Value	CI (%)	Value	CI (%)	Value	CI (%)
$\mu_{maxVFA}$	0.14	46	0.10	151	0.05	157	0.003	9234
$K_{ace}$	1.56	4	1.03	15	0.82	19	27.3	1
$K_{prop}$	60.85	1	0.56	28	0.22	33	0.000	3723191
$K_{but}$	–	–	–	–	–	–	3552	0,01
$Ki_{ace}$	–	–	0.24	65	–	–	0.004	7455
$Ki_{prop}$	–	–	–	–	0.10	74	0.007	4448
$C_{ace}$	0.66	10	0.88	18	–	–	56.76	1
$C_{prop}$	2.00	1	–	–	0.90	8	61.15	1
$C_{but}$	–	–	0.35	45	18.86	10	40709	0.001
J	0.24	–	0.40	–	0.23	–	17.5	–

**Table 5**  
Kinetic structures to describe the assimilations of multiple VFAs by *Rs. rubrum* when acetate and propionate are considered as one sole substrate.

	Carbon source 1	Carbon source 2
Mix acetate and propionate Case A.3	$\varphi_1 = X \cdot \mu_{maxAce+Prop} \frac{[Ace] + [Prop]}{K_{Ace+Prop} + [Ace] + [Prop]}$	
Mix acetate propionate and butyrate Case D.3	$\varphi_1 = X \cdot \mu_{max3VFA} \frac{[Ace] + [Prop]}{K_{Ace+Prop} + [Ace] + [Prop]}$	
	<b>Carbon source 3</b>	
	$\varphi_2 = X \cdot \mu_{max3VFA} \frac{[But]}{K_{But} + [But]}$	
	$\frac{[Prop] + [Ace]}{Ki_{Prop+Ace} + [Ace] + [Prop]}$	

**Table 6**  
Parameter estimations and their confidence intervals for several models describing the assimilations of VFA mixtures when acetate and propionate are considered as one substrate.

	Mix acetate and propionate (A.3)		Mix acetate propionate and butyrate (D.3)	
	Value	CI (%)	Value	CI %
$\mu_{maxVFA}$	0.47	29	2.61	4
$K_{VFA}$	10.98	1	67.14	0.2
$K_{but}$	–	–	94.87	0.1
$Ki_{ace+Prop}$	–	–	0.025	491
$C_{VFA}$	1.08	13	0.95	10
$C_{but}$	–	–	1.36	7
J	0.086	–	0.33	–

parameter estimation.

The best models were cross-validated using a data set obtained from an independent experiment. In the following, each state prediction is

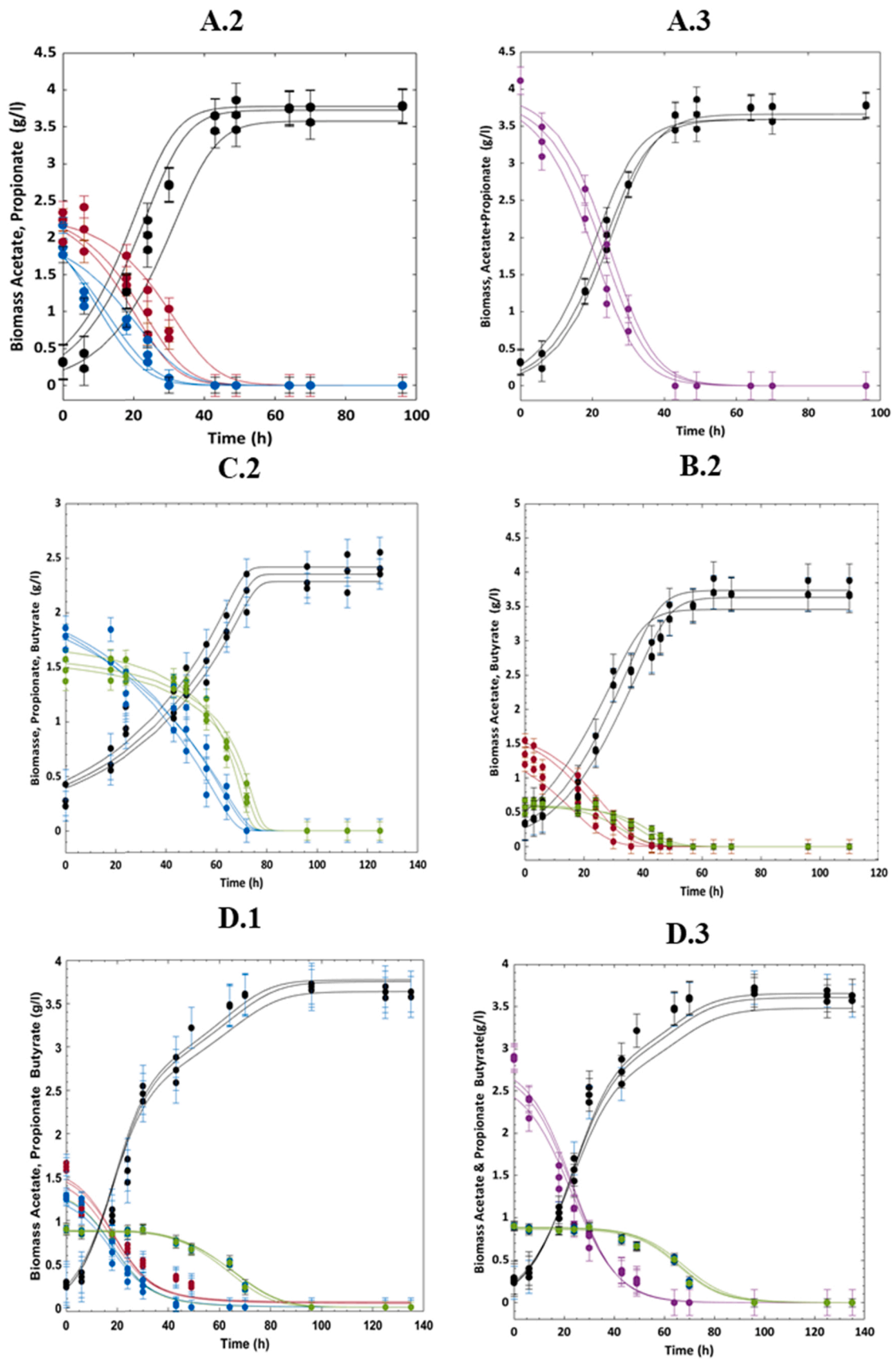


Fig. 5. Experimental monitoring (dot) and simulated value (line), of biomass growth(●), acetate (●), propionate(●), and butyrate (●) consumptions in cultures of *Rs. rubrum* S1H. The substrate shown in (●) is composed of acetate and propionate. The bars represent the confidence intervals at 95 % calculated from the a posteriori measurement error variance from (6).

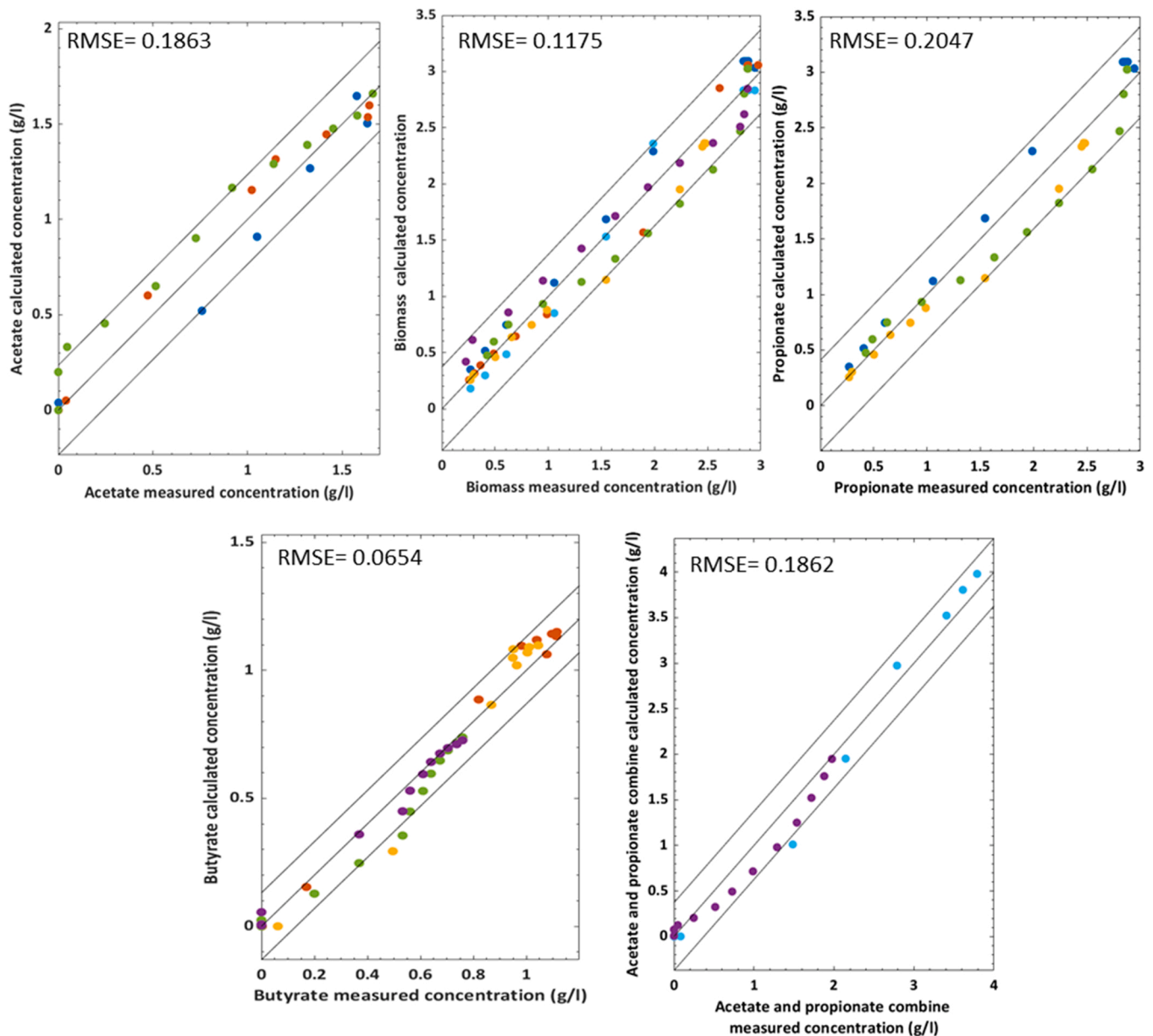


Fig. 6. Correlation between model predictions and measured data for each case scenario describing the assimilation of mixtures of VFAs by *Rs. rubrum*. Each color represents a specific case as follows: Case A.2(●), Case A.3 (●), Case B.2(●), Case C.2 (●), Case D.1(●), Case D.3 (●).

quantitatively assessed by its RMSE (Fig. 6). The resulting small values confirm the good predictive capability of the model whatever the considered substrate combination. It can also be noticed that all predicted state trajectories are included in the 95 % confidence intervals. The mixture of 3 VFAs as carbon source however shows the lowest predictive capability and parameter sensitivity. The development of those models brought a precise representation of multiple VFA uptakes by *Rs. rubrum* and in particular the different inhibition phenomena via a kinetic structure based on inhibition factors. In addition, the best representation is obtained when the assimilation occurs via the same pathway. Those macroscopic models present an added explicative value for the process in addition to a predictive capacity and, by extension, could serve as a digital twin basis for process control and optimization [34,35]. Those models could also be useful in the development of software sensors for online VFA monitoring based on biomass measurement to ensure maximal biomass growth rate or prevent accumulation at

inhibitory levels of implied metabolites.

#### 4. Conclusion

To better understand and control processes involving several VFAs, macroscopic mechanistic models were developed in *Rs. rubrum*, to provide an accurate prediction of substrate competition occurring when a mixture of acetate, propionate, and butyrate is used in cultures of *Rs. rubrum*. The good predictive capability of the proposed models and the related parameter accuracy, independently of the VFA mixture content, are quite encouraging and these satisfactory results, therefore, open the door to a better design and operation of PNSB-based industrial biotechnology for resource recovery, enabling high overall VFA assimilation efficiencies without jeopardizing the overall process rates.

## Funding sources

This work was supported by the Belgian Fund for Scientific Research (Grand Equipment-F.R.S-FNRS); the Concerted Research Action ARC project [P. Cabecas, PHASYN, 2017]; the CDR -FNRS [B. Leroy, Redox homeostasis in purple bacteria]; the Research Foundation Flanders [A. Alloul, 12W0522N]; the European Union's Horizon 2020 Research and Innovation program on project 'Saraswati 2.0' [2020,821427], the IOF via project PurpleRace [A. Alloul, 40207].

## CRedit authorship contribution statement

PCB, performed part of the experiments, elaborated the model and drafted the paper; QDM, performed part of the experiments AA, performed part of the experiments and participated to the writing of the paper, AT and RO participate to the analytics, SEV designed part of the experiments and to the writing of the paper, AVW participated to the model elaboration and the writing of the paper, RW cosupervised the work and participated to the writing of the paper, LD cosupervised the work and participated to the elaboration of the model and the writing of the paper; BL designed and supervised the study and participated to the writing of the paper.

## Declaration of Competing Interest

The authors declare that they have no known competing financial interests or personal relationships that could have appeared to influence the work reported in this paper.

## Appendix A. Supporting information

Supplementary data associated with this article can be found in the online version at [doi:10.1016/j.bej.2022.108547](https://doi.org/10.1016/j.bej.2022.108547).

## References

- [1] G. Moretto, F. Valentino, P. Pavan, M. Majone, D. Bolzonella, Optimization of urban waste fermentation for volatile fatty acids production, *Waste Manag.* 92 (2019) 21–29.
- [2] F. Valentino, G. Moretto, L. Lorini, D. Bolzonella, P. Pavan, M. Majone, Pilot-scale polyhydroxyalkanoate production from combined treatment of organic fraction of municipal solid waste and sewage sludge, *Ind. Eng. Chem. Res.* 58 (2019) 12149–12158, <https://doi.org/10.1021/acs.iecr.9b01831>.
- [3] W. Verstraete, P. Clauwaert, S.E. Vlaeminck, Used water and nutrients: recovery perspectives in a 'panta rhei' context, *Bioresour. Technol.* 215 (2016) 199–208.
- [4] D.-H.H. Kim, J.-H.H. Lee, Y. Hwang, S. Kang, M.-S.S. Kim, Continuous cultivation of photosynthetic bacteria for fatty acids production, *Bioresour. Technol.* 148 (2013) 277–282, <https://doi.org/10.1016/j.biortech.2013.08.078>.
- [5] J.C. Fradinho, A. Oehmen, M.A.M. Reis, Photosynthetic mixed culture polyhydroxyalkanoate (PHA) production from individual and mixed volatile fatty acids (VFAs): substrate preferences and co-substrate uptake, *J. Biotechnol.* 185 (2014) 19–27, <https://doi.org/10.1016/j.jbiotec.2014.05.035>.
- [6] A. Alloul, S. Wuyts, S. Lebeer, S.E. Vlaeminck, Volatile fatty acids impacting phototrophic growth kinetics of purple bacteria: paving the way for protein production on fermented wastewater, *Water Res.* 152 (2019) 138–147, <https://doi.org/10.1016/j.watres.2018.12.025>.
- [7] M.-F. Dignac, P. Ginestet, D. Rybacki, A. Bruchet, V. Urbain, P. Scribe, Fate of wastewater organic pollution during activated sludge treatment: nature of residual organic matter, *Water Res.* 34 (2000) 4185–4194, [https://doi.org/10.1016/S0043-1354\(00\)00195-0](https://doi.org/10.1016/S0043-1354(00)00195-0).
- [8] A. Alloul, R. Ganigué, M. Spiller, F. Meerburg, C. Cagnetta, K. Rabaey, S. E. Vlaeminck, Capture–ferment–upgrade: a three-step approach for the valorization of sewage organics as commodities, *Environ. Sci. Technol.* 52 (2018) 6729–6742, <https://doi.org/10.1021/acs.est.7b05712>.
- [9] S.-J. Lim, B.-J. Kim, C.-M. Jeong, Y.H. Ahn, H.N. Chang, Anaerobic organic acid production of food waste in once-a-day feeding and drawing-off bioreactor, *Bioresour. Technol.* 99 (2008) 7866–7874.
- [10] K. Komemoto, Y.G. Lim, N. Nagao, Y. Onoue, C. Niwa, T. Toda, Effect of temperature on VFA's and biogas production in anaerobic solubilization of food waste, *Waste Manag.* 29 (2009) 2950–2955.
- [11] P. Zhang, Y. Chen, Q. Zhou, Waste activated sludge hydrolysis and short-chain fatty acids accumulation under mesophilic and thermophilic conditions: effect of pH, *Water Res.* 43 (2009) 3735–3742.
- [12] J. Jiang, Y. Zhang, K. Li, Q. Wang, C. Gong, M. Li, Volatile fatty acids production from food waste: Effects of pH, temperature, and organic loading rate, *Bioresour. Technol.* 143 (2013) 525–530, <https://doi.org/10.1016/j.biortech.2013.06.025>.
- [13] W.S. Lee, A.S.M. Chua, H.K. Yeoh, G.C. Ngoh, A review of the production and applications of waste-derived volatile fatty acids, *Chem. Eng. J.* 235 (2014) 83–99.
- [14] S. Dahiya, O. Sarkar, Y.V. Swamy, S.V. Mohan, Acidogenic fermentation of food waste for volatile fatty acid production with co-generation of biohydrogen, *Bioresour. Technol.* 182 (2015) 103–113.
- [15] H. Brandl, R.A. Gross, R.W. Lenz, R. Lloyd, R.C. Fuller, The accumulation of poly(3-hydroxyalkanoates) in *Rhodobacter sphaeroides*, *Arch. Microbiol.* 155 (1991) 337–340, <https://doi.org/10.1007/bf00243452>.
- [16] H. Brandl, E.J. Knee, R.C. Fuller, R.A. Gross, R.W. Lenz, Ability of the phototrophic bacterium *Rhodospirillum rubrum* to produce various poly( $\beta$ -hydroxyalkanoates): potential sources for biodegradable polyesters, *Int. J. Biol. Macromol.* 11 (1989) 49–55, [https://doi.org/10.1016/0141-8130\(89\)90040-8](https://doi.org/10.1016/0141-8130(89)90040-8).
- [17] J.M.L. Dias, A. Oehmen, L.S. Serafim, P.C. Lemos, M.A.M. Reis, R. Oliveira, Metabolic modelling of polyhydroxyalkanoate copolymers production by mixed microbial cultures, *BMC Syst. Biol.* 2 (2008) 59.
- [18] Y. Jiang, M. Heby, R. Kleerebezem, G. Muyzer, M.C.M. van Loosdrecht, Metabolic modeling of mixed substrate uptake for polyhydroxyalkanoate (PHA) production, *Water Res.* 45 (2011) 1309–1321, <https://doi.org/10.1016/j.watres.2010.10.009>.
- [19] L. Marang, Y. Jiang, M.C.M. van Loosdrecht, R. Kleerebezem, Butyrate as preferred substrate for polyhydroxybutyrate production, *Bioresour. Technol.* 142 (2013) 232–239.
- [20] J. Tamis, L. Marang, Y. Jiang, M.C.M. van Loosdrecht, R. Kleerebezem, Modeling PHA-producing microbial enrichment cultures—towards a generalized model with predictive power, *N. Biotechnol.* 31 (2014) 324–334.
- [21] X. Wang, G. Carvalho, M.A.M. Reis, A. Oehmen, Metabolic modeling of the substrate competition among multiple VFAs for PHA production by mixed microbial cultures, *J. Biotechnol.* 280 (2018) 62–69.
- [22] H.L. Korneberg, H.A. Krebs, Synthesis of cell constituents from C2-units by a modified tricarboxylic acid cycle, *Nature* 179 (1957) 988–991, <https://doi.org/10.1038/179988a0>.
- [23] T.J. Erb, I.A. Berg, V. Brecht, M. Müller, G. Fuchs, B.E. Alber, Synthesis of C5-dicarboxylic acids from C2-units involving crotonyl-CoA carboxylase/reductase: the ethylmalonyl-CoA pathway, *Proc. Natl. Acad. Sci.* 104 (2007) 10631–10636.
- [24] B. Leroy, Q. De Meur, C. Moulin, G. Wegria, R. Wattiez, New insight into the photoheterotrophic growth of the isocitrate lyase-lacking purple bacterium *Rhodospirillum rubrum* on acetate, *Microbiology* 161 (2015) 1061–1072, <https://doi.org/10.1099/mic.0.000067>.
- [25] K. Schneider, R. Peyraud, P. Kiefer, P. Christen, N. Delmotte, S. Massou, J.-C. Portais, J.A. Vorholt, The ethylmalonyl-CoA pathway is used in place of the glyoxylate cycle by *Methylobacterium extorquens* AM1, during growth on acetate, *J. Biol. Chem.* 287 (2012) 757–766.
- [26] M. Knight, The photometabolism of propionate by *Rhodospirillum rubrum*, *Biochem. J.* 84 (1962) 170.
- [27] Q. De Meur, A. Deutschbauer, M. Koch, G. Bayon-Vicente, P. Cabecas Segura, R. Wattiez, B. Leroy, New perspectives on butyrate assimilation in *Rhodospirillum rubrum* SIH under photoheterotrophic conditions, *BMC Microbiol.* (2020) 1–20.
- [28] Q. De Meur, A. Deutschbauer, M. Koch, R. Wattiez, B. Leroy, Genetic plasticity and ethylmalonyl coenzyme A pathway during acetate assimilation in *Rhodospirillum rubrum* SIH under photoheterotrophic conditions, *Appl. Environ. Microbiol.* 84 (2018) e02038–17.
- [29] L. Segers, W. Verstraete, Conversion of organic acids to H<sub>2</sub> by *Rhodospirillaceae* grown with glutamate or dinitrogen as nitrogen source, *Biotechnol. Bioeng.* 25 (1983) 2843–2853.
- [30] M. Suhaimi, J. Liessens, W. Verstraete, NH<sub>4</sub><sup>+</sup>/4-N assimilation by *Rhodobacter capsulatus* ATCC 23782 grown axenically and non-axenically in N and C rich media, *J. Appl. Bacteriol.* 62 (1987) 53–64.
- [31] ESA, Engineering of the waste compartment - ESA contract 15689/01/NL/ND TECHNICAL NOTE 71.9.4 – Confidential report, 2005.
- [32] P. Cabecas Segura, Q. De Meur, A. Tanghe, R. Onderwater, L. Dewasme, R. Wattiez, B. Leroy, Effects of mixing volatile fatty acids as carbon sources on *Rhodospirillum rubrum* carbon metabolism and redox balance mechanisms, *Microorg* 9 (2021), <https://doi.org/10.3390/microorganisms9091996>.
- [33] R.K. Clayton, Photosynthetic metabolism of propionate in *Rhodospirillum rubrum*, *Arch. Mikrobiol.* 26 (1957) 29–31.
- [34] J.H. Lee, Model predictive control: Review of the three decades of development, *Int. J. Control. Autom. Syst.* 9 (2011) 415–424.
- [35] S.J. Qin, T.A. Badgwell, A survey of industrial model predictive control technology, *Control Eng. Pract.* 11 (2003) 733–764.